

Analytical Model for Gaussian Disorder Traps in Organic Thin-Film Transistor

Qiusong Chen,^{1, a)} Juan E. Sanchez,² Dong Lin,³ Yanlian Lei,⁴ and Guodong Zhu^{1, b)}

¹⁾Department of Materials Science, Fudan University, Shanghai 200433, China

²⁾DEVSIM LLC, PO Box 50096, Austin, TX 78763, USA

³⁾College of Information Engineering, Jimei University, Xiamen 361021, China

⁴⁾School of Physical Science and Technology, Southwest University, Chongqing 400715, China

(Dated: 30 June 2021)

Structural defects and chemical impurities exist in organic semiconductors acting as trap centers for the excited states. This work presents a novel analytical model to calculate the trapping and detrapping rates between two Gaussian density of states. Miller-Abrahams rate and Fermi-Dirac statistics are employed in this model. The introduction of effective filled and empty sites for correlated bands greatly simplifies the expression of recombination rate. A technology computer-aided design simulator-DEVSIM was used to simulate the donor-like traps in an organic semiconductor DPP-DTT based thin-film transistor, showing good agreement with the measured transfer characteristic.

I. INTRODUCTION

Organic semiconductors are a class of promising materials for high-efficiency¹, low-cost², flexible³, and multifunctional⁴ electronic devices. The trap states induced by the chemical impurities and structural defects in organic semiconductors play a critical role in electric performance.

For example, chemical impurities have been doped in host materials as guest molecules to improve the electroluminescence in light-emitting diodes^{5,6} and to enhance the light absorption efficiency in dye sensitized solar cells^{7,8}. Other reports directly utilized the physics of trap states to build memories and sensors⁹⁻¹¹.

However, the applications of organic semiconducting materials in different areas are restricted by the trap states for the following two reasons: 1) the traps can serve as unintentional recombination centers in light-emitting diodes and solar cells^{12,13}, 2) carrier transport is also localized by chemical impurities and structural defects, resulting in carrier mobilities far below the theoretical prediction^{14,15}. The study of trap related mechanisms is therefore crucial in extracting theoretical performance limits of organic semiconductors. Still many questions and challenges need to be addressed before engineering high-performance electronic devices.

In order to clarify the underlying mechanisms of trap related physics, several numerical methods have been proposed. The simplest approach included several discrete energy depths for traps, assuming that the trapping and detrapping rates are standard first order differential equations with time^{16,17}. However, the trap states in organic semiconductors are dominated by continuous energy distributions^{11,18}. Several works employed Gaussian distribution of exponential functions for trap levels to an-

alyze the field-induced detrapping and thermal aging effects in organic semiconductors^{17,19,20}. These works were mostly based on the master equation approach or Monte Carlo simulation^{19,21}. However, both approaches are time-consuming methods for device simulation¹⁹. Hence, a more efficient and versatile approach is desired to explore the trap related kinetics.

In this study, we demonstrate a new method to analyze the charge generation (trapping) and recombination (detrapping) rate between two Gaussian density of states (DOS), by combining the Fermi-Dirac statistics with Miller-Abrahams equation²². Two variables of effective filled site (EFS) and effective empty site (EES) are defined in the expression of detrapping rate to simplify the algorithm complexity. Then, this method is applied to the understanding of the highest occupied molecular orbit (HOMO) and the donor-like trap (DLT) states in a Poly[2,5-(2-octyldodecyl)-3,6-diketopyrrolopyrrole-alt-5,5-(2,5-di(thien-2-yl)thieno [3,2-b]thiophene)] (DPP-DTT)²³ based organic thin-film transistor (OTFT). The simulated results demonstrated by a technology computer-aided design (TCAD) platform of DEVSIM²⁴ show good agreement with the measured transfer characteristic. This model can also be applied to other types of traps in organic electronic materials, such as acceptor-like traps.

II. MODELING

In both organic and inorganic materials, the energetic distribution of trap states is typically approximated by a Gaussian function with a standard energetic deviation or an exponential function with a modified characteristic temperature^{11,18,20,25,26}. The Gaussian function is a better choice to describe the limited nature of trap density.

Because of the less crystallized structure in organic materials, the energetic disorder of conductive bands in organic semiconductors are typically also given by Gaussian DOS²⁷. Unlike the inorganic crystalline structure, there is no clear boundary between the allowed band

^{a)}Also at School of Physics and Electronic Science, Guizhou Education University, 115 Gaixin Road, Guiyang 550018, China

^{b)}Electronic mail: gdzhu@fudan.edu.cn

and the forbidden band²⁸. Boltzmann statistics is therefore not a proper approximation for the states in amorphous organic semiconductors²⁸ and Fermi-Dirac statistics should be employed to calculate the average number in a single-particle state²⁹.

The charge transition model, including trapping and detrapping, between various energy levels in organic semiconductors must be treated differently from inorganic crystals. In the following context, we employ Gaussian DOS to describe energy statistics for both of HOMO and DLT, and then use Miller-Abrahams rate and Fermi-Dirac statistics to describe the charge transition between these two energy levels.

A. The Gaussian DOS for HOMO and DLT

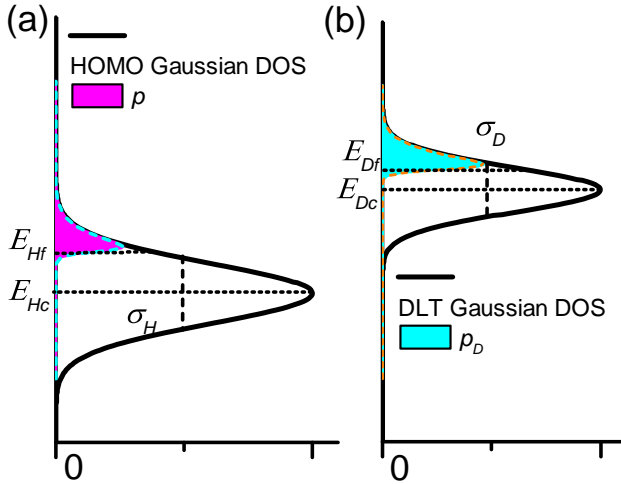


FIG. 1. The diagrams of filling states in Gaussian DOS for HOMO and DLT

The Gaussian DOS for HOMO (g_H) of organic materials is as follows :

$$g_H(E_H, E_{Hc}, \sigma_H) = \frac{N_H}{\sigma_H \sqrt{2\pi}} \exp\left(-\frac{(E_H - E_{Hc})^2}{2\sigma_H^2}\right) \quad (1)$$

where E_H is an energy level of a specific state in HOMO. N_H , σ_H , and E_{Hc} are the total density, the distribution width, and energy center of HOMO DOS, respectively. In the following content, we will use $g_H(E_H)$ as a shorthand for $g_H(E_H, E_{Hc}, \sigma_H)$.

The black solid curve in Fig. 1(a) represents the Gaussian distribution for HOMO DOS and the empty sites in it. In addition, a hole is defined to be the remaining delocalized positive charge after an electron escapes from a HOMO site, whose density is:

$$p = \int_{-\infty}^{\infty} g_H(E_H, E_{Hc}, \sigma_H) (1 - f(E_H, E_f)) dE_H \quad (2)$$

in which $f(E, E_f)$ is Fermi-Dirac statistics and it reads:

$$f(E, E_f) = \frac{1}{e^{\frac{(E - E_f)}{k_B T}} + 1} \quad (3)$$

where E_f , k_B , T are Fermi energy level, Boltzmann's constant, and the absolute temperature, respectively.

It should be noted that, only in the equilibrium state, different bands in the system share the same Fermi level. Otherwise, in the non-equilibrium state, every band has its own Fermi level to describe the overall occupation of the sites³⁰. In such condition, this energy level is termed as quasi Fermi level. As the trapping and detrapping processes typically occur in a non-equilibrium state, we should use quasi Fermi level of different bands in the following context, i.e. E_{Hf} for HOMO and E_{Df} for DLT.

The trapped charges consist of both donor-like and acceptor like states across the forbidden energy gap³¹. Then, the DOS for deep-level DLT is in the same manner of Gaussian distribution:

$$g_D(E_D, E_{Dc}, \sigma_D) = \frac{N_D}{\sigma_D \sqrt{2\pi}} \exp\left(-\frac{(E_D - E_{Dc})^2}{2\sigma_D^2}\right) \quad (4)$$

where E_D is an energy level of a specific state in DLT. N_D , σ_D , and E_{Dc} are the total density, the distribution width, and energy center of DLT DOS, respectively. In the following content, we will use $g_D(E_D)$ as a shorthand for $g_D(E_D, E_{Dc}, \sigma_D)$.

The black solid curve in Fig. 1(b) represents the Gaussian distribution for DLT and the empty sites in it. Since the DLT site is neutral if occupied by an electron and positively charged if empty, the density of trapped charge corresponds to the empty sites. Then the trap density reads:

$$p_D = \int_{-\infty}^{\infty} g_D(E_D, E_{Dc}, \sigma_D) (1 - f(E_D, E_{Df})) dE_D \quad (5)$$

B. Miller-Abrahams Equation

To describe the transition rate of electrons from one site with energy level of E_i to another site with E_j , we employ Miller-Abrahams rate^{19,22}, which reads:

$$v_{ij} = v_0 \exp\left(-2\frac{R_{ij}}{a_i} - \frac{E_j - E_i + |E_j - E_i|}{2k_B T}\right) \quad (6)$$

where v_0 is attempt frequency, a_i is the localization scale of initial state, R_{ij} is the distance between both states.

C. Trapping Process

For the trapping process, the electron jumps from a neutral DLT site to an empty HOMO site. Here, we assume that all states of DLT are higher than HOMO, because Gaussian distributed DLT are deep-level bands³¹.

Then by integrating the transition rates of all electrons in DLT to all empty site in HOMO, we can get the total rate of trapping. Fig. 2 exhibits this process. Hence, the overall trapping rate reads:

$$k_T = \int \int_{-\infty}^{\infty} v_{DH} g_D(E_D) f(E_D, E_{Df}) g_H(E_H) (1 - f(E_H, E_{Hf})) dE_D dE_H \quad (7)$$

where E_D, E_H are two energy sites located on DLT and HOMO, respectively. v_{DH} is Miller-Abrahams rate for electron transition form site of E_D to E_H . It reads :

$$v_{DH} = v_0 \exp(-2\alpha_D R_{DH}) \quad (8)$$

where α_D is the inverse localization scale of DLT site, R_{DH} is the average distance from HOMO sites to DLT sites.

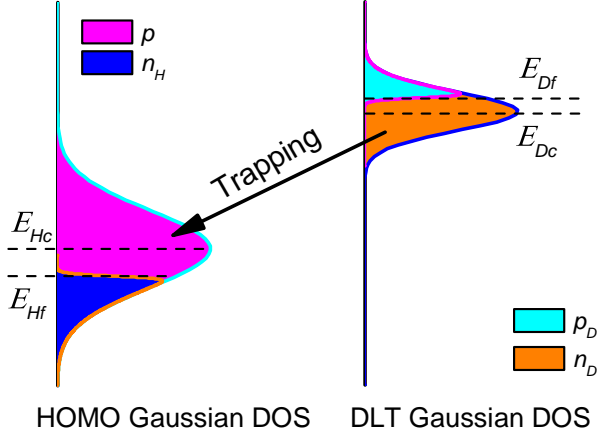


FIG. 2. The diagrams of electron's trapping process from the neutral sites in DLT to the empty sites in HOMO. p and n_H are the empty sites(holes) and the filled sites in HOMO DOS. n_D and p_D denote the filled and the empty sites in DLT DOS

After separating variables, the above expression can be simplified as:

$$k_T = v_{DH} n_D p \quad (9)$$

in which n_D is the filled sites in DLT. It is illustrated as the orange area in Fig. 2 and reads:

$$n_D = \int_{-\infty}^{\infty} g_D(E_D, E_{Dc}, \sigma_D) f(E_D, E_{Df}) dE_D = N_D - p_D \quad (10)$$

D. Detrapping Process

For the detrapping process, the electron jumps from a filled HOMO site to an empty DLT site as indicated by

the red solid arrow in Fig. 3. Then by integrating all electrons in HOMO to all empty sites in DLT, we can get the total rate of detrapping. So the detrapping rate reads:

$$k_D = \int \int_{-\infty}^{\infty} v_{HD} g_H(E_H) f(E_H, E_{Hf}) g_D(E_D) (1 - f(E_D, E_{Df})) dE_H dE_D \quad (11)$$

where v_{HD} is Miller-Abrahams rate for electron's transition form the site of E_H in HOMO to E_D in DLT. v_{HD} reads:

$$v_{HD} = v_0 \exp\left(-2\frac{R_{DH}}{a_H} - \frac{E_D - E_H}{k_B T}\right) \quad (12)$$

where a_H is the average localization scale of HOMO site. Using the following replacement:

$$v_{HD0} = v_0 \exp(-2\alpha_H R_{DH}) \quad (13)$$

the expression of Eq. (11) can be rewritten as :

$$k_D = \int \int_{-\infty}^{\infty} v_{HD0} \exp\left(-\frac{E_D - E_H}{k_B T}\right) g_H(E_H) f(E_H, E_{Hf}) g_D(E_D) (1 - f(E_D, E_{Df})) dE_H dE_D \quad (14)$$

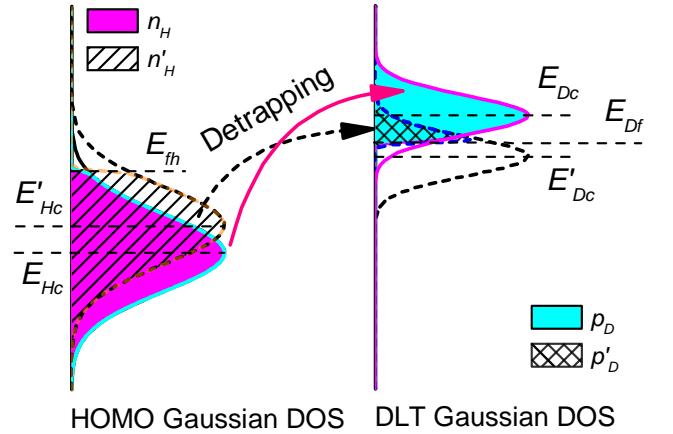


FIG. 3. The diagrams of electron's detrapping process from HOMO to the empty sites in DLT. n_H is the actual filled sites and n'_H is the effective filled sites in HOMO. p_D is actual empty sites and p'_D is the effective empty sites in DLT

E. Effective Empty and Filled Sites

Eq. (14) has one more exponential terms than Eq. (7), but it can still be simplified by the method of separation of variables. Here, we define two parameters of E'_{Hc} and E'_{Dc} as effective energy centers for HOMO and

DLT DOS, respectively. The expressions of two effective energy centers are:

$$E'_{Hc} = E_{Hc} + \frac{\sigma_H^2}{k_B T} \quad (15)$$

$$E'_{Dc} = E_{Dc} - \frac{\sigma_D^2}{k_B T} \quad (16)$$

Fig. 3 illustrate the energy shift of E'_{Hc} and E'_{Dc} with respect to E_{Hc} and E_{Dc} , respectively. By introducing effective energy centers for both HOMO and DLT levels, Eq. (14) can be rewritten as :

$$k_D = c_E v_{DH} \int_{-\infty}^{\infty} g_H(E_H, E'_{Hc}, \sigma_H) f(E_H, E_{Hf}) g_D(E_D, E'_{Dc}, \sigma_D) (1 - f(E_D, E_{Df})) dE_H dE_D \quad (17)$$

in which c_E reads:

$$c_E = \exp\left(\frac{\sigma_H^2 + \sigma_D^2}{2k_B^2 T^2} + \frac{E_{Hc} - E_{Dc}}{k_B T}\right) \quad (18)$$

Compared with Eq. (7), Eq. (17) can also be simplified to a product form like Eqs. (9):

$$k_D = c_E v_{DH} n'_H p'_D \quad (19)$$

in which n'_H reads:

$$n'_H = \int_{-\infty}^{\infty} g_H(E_H, E'_{Hc}, \sigma_H) f(E_H, E_{Hf}) dE_H \quad (20)$$

and p'_D reads:

$$p'_D = \int_{-\infty}^{\infty} g_D(E_D, E'_{Dc}, \sigma_D) (1 - f(E_D, E_{Df})) dE_D \quad (21)$$

Because Eqs. (20) and (21) are similar to Eqs. (10) and (5), respectively, we define n'_H as EFS for HOMO and p'_D as EES for DLT.

So far, we used both Fermi-Dirac statistics and Miller-Abrahams equation to derive the trapping and detrapping rates of DLT in the Gaussian energetic disorder semiconductors. The calculation complexity caused by the barrier in the detrapping process was reduced by virtue of introducing EFS and EES for the correlated bands. Then the detrapping rate is simplified from a sophisticated integral expression (Eq. (11)) to a concise product form (Eq. (19)). The black dot arrow in Fig. 3 indicates the simplified detrapping picture. In the following section, we will analyze the relationship between different parameters and variables in this model. Then, this model was employed to simulate a DPP-DTT based transistor with a bottom-gate/ top-contact configuration.

III. DATA ANALYSIS

A. Parameters and Variables

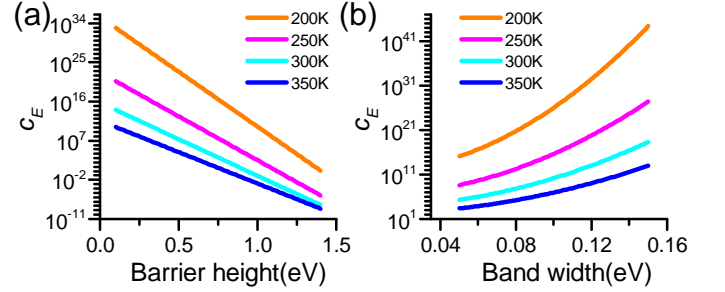


FIG. 4. (a) Dependencies of c_E on barrier height ($E_{Dc} - E_{Hc}$) at various temperature. All Gaussian widths for these lines are fixed at 0.11 eV. (b) Dependencies of c_E on one band width of Gaussian HOMO or DLT DOS at various temperature. The barrier height for these curves are set to 0.25 eV.

In the above content, the trapping and detrapping rates are reduced to the product forms in Eq. (9) and (19). The coefficient v_{DH} for trapping in Eq. (9) reflects the impacts of orbit localization in DLT and spacial distance from HOMO to DLT. The other two variables are the filled electrons in DLT (n_D) and the empty sites in HOMO (p). But for the detrapping rate, there's an extra coefficient of c_E in Eq. (19). Fig. 4 (a) and (b) present the dependence of c_E on the barrier height and the band width of Gaussian DOS. In Fig. 4 (a), c_E shows a dramatically exponential decay with respect to the barrier height between the Gaussian centers of HOMO and DLT. This feature intuitively describes the physical role of energy barrier. However, there are two results to note: ①, most of c_E values within the range shown in Fig. 4 is greater than 1; ② the range of c_E decreases with device temperature for in both Fig. 4 (a) and (b). Both results are inconsistent with Miller-Abrahams rate in Eq. (6), because the detrapping rate should be reduced by the energy barrier ($c_E < 1$) and enhanced with higher temperature. So, the attenuation effect of the potential barrier on detrapping process will act more on EES and EFS. in Eq. (19).

Fig. 5 presents the dependence of EES and EFS on the actual charge density of n_H in HOMO and p_D in DLT, respectively. These data are obtained by Paasch's method about the Gauss-Fermi integral²⁷. It can be observed from Fig. 5 (a) that the n'_H relationship with the n_H asymptotically reaches a slope equal to 1 in the log-log plot for small densities. And, the p'_D relationship with the p_D presents the same manner. In this region, the values of n'_H and p'_D are 5 ~ 15 orders of magnitude smaller than n_H and p_D , respectively. The magnitude of difference increases with the Gaussian DOS widths, because the energy shift of E'_{Hc} and E'_{Dc} increases with these two widths in Eqs. (15) and (16). However, these magnitude

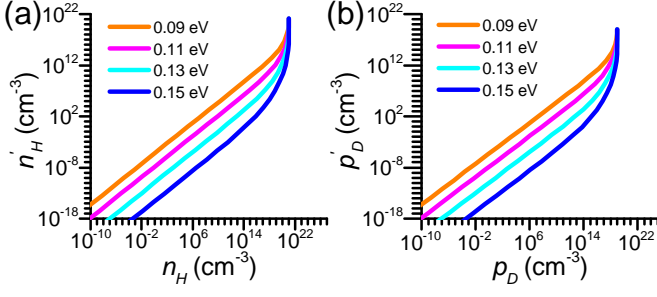


FIG. 5. (a) Dependencies of n'_H on n_H of various band width for Gaussian HOMO DOS at 300K. (b) Dependencies of p'_D on p_D for various band width of Gaussian DLT DOS at 300K. The total density for HOMO and DLT DOS are $1.2 \times 10^{21} \text{ cm}^{-3}$ and $1.0 \times 10^{19} \text{ cm}^{-3}$, respectively.

differences decrease when n_H and p_D become saturated. So the slop of these curves becomes very steep in these regions in both Fig. 5 (a) and (b). Such phenomenon reflects the saturation characteristic of the Gaussian distribution. Take the Gaussian HOMO DOS as example, the quasi Fermi level is the only variable of EFS' expression in Eq. (21). So, while the actual filled sites in HOMO DOS are saturated, the raised effective energy center of E'_{Hc} makes EFS increase obviously.

B. TCAD Simulation for OTFT

In organic semiconductors, the surface trap density is more prominent than the bulk trap density. A device with active region on the surface is therefore an appropriate application to validate this method. And OTFT meets this criteria, because the conductive channel is located in the interface area of semiconductors.

In the following content, we demonstrate our model in a TCAD simulation of an OTFT device with the bottom-gate/top-contact configuration. The simulation parameters and device dimensions are listed in Table I. The DEVSIM²⁴ TCAD simulator was employed to realize a finite volume method (FVM) analysis. The typical TCAD approach of drift-diffusion model solves three equations:

The Poisson equation:

$$-\nabla \cdot (\epsilon_r \epsilon_0 \nabla \psi) = e \cdot (p - n + p_D) \quad (22)$$

where ψ is electrical potential, ϵ_0 is the permittivity of vacuum, ϵ_r is the relative permittivity of the organic material, and e is the elementary charge.

Hole Continuity Equation:

$$\frac{\partial p}{\partial t} = \nabla \cdot (p \mu_p \nabla \psi + D_p \nabla p) + G_p \quad (23)$$

where μ_p , D_p and G_p are the mobility, diffusion coefficient and net generation rate for holes, respectively.

Electron Continuity Equation:

$$\frac{\partial n}{\partial t} = \nabla \cdot (-n \mu_n \nabla \psi + D_n \nabla n) + G_n \quad (24)$$

where μ_n , D_n and G_n are the mobility, diffusion coefficient and net generation rate of electrons, respectively.

To calculate the variance of DLT density over time, an extra equation for the net generation rate of DLT is solved simultaneously with the above three equations. The net generation rate of DLT reads:

$$\frac{\partial q_D}{\partial t} = k_T - k_D \quad (25)$$

TABLE I. The parameters used to simulate the DPP-DTT based OTFT if not explicitly stated elsewhere.

Model	Symbol	Value	Unit
Device temperature	T	300	K
Total density for HOMO ³²	N_H	1.2×10^{21}	cm^{-3}
HOMO DOS width ^{29,30}	σ_H	0.13	eV
HOMO DOS center ³³	E_{Hc}	-5.2	eV
LUMO DOS center ³³		-3.5	ev
Total density for DLT ¹¹	N_{Ds}	1.0×10^{13}	cm^{-2}
DLT DOS width	σ_D	0.11	eV
DLT DOS center	E_{Dc}	3.81	eV
Trap thickness	d_D	3	nm
Average distance between HOMO and DLT	R_{DH}	5	nm
Localization length for HOMO and DLT ¹⁹	a_i	0.5	nm
Attempt frequency ¹⁹	ν_0	1	s^{-1}
DPP-DTT thickness		40	nm
Insulator's thickness		300	nm
OTFT channel length		100	μm
Relative permittivity for DPP-DTT	ϵ_{r_Semi}	4	
Relative permittivity for Insulator SiO ₂	$\epsilon_{r_SiO_2}$	3.9	
Thermionic emission velocity at source and drain ³⁴		10^7	cm/s

As our method is based on the bulk density of DLT, we convert the total surface trap density to the total bulk density through an exponential decay relationship with depth:

$$N_D = \frac{N_{Ds}}{d_D} \exp\left(-\frac{x}{d_D}\right) \quad (26)$$

where x is the depth from the insulator-semiconductor interface to the semiconducting layer, d_D is the characteristic thickness of DLT. The values for these parameters are listed in Table I. Integrating Eq. (26) on the depth in

semiconductor layer, the sum of bulk density is consistent with surface density.

Here, we assume there is only one kind of trap. So, in Eq. (22), the total charges in Poisson's equation include three parts: holes, electrons and DLT. As the organic OTFT works in the accumulation regime for on-state and depletion regime for off-state, we take only the electron's transition between HOMO and DLT in consideration. Then, we can get the following two results:

$$G_p = -(k_T - k_D) \quad (27)$$

$$G_n = 0 \quad (28)$$

For the carriers transport, we use the macroscopic conductivity model for holes^{15,35} and Poole-Frenkel model for electrons³¹. Then, a typical model for Schottky contacts is considered on source and drain³⁶. The thermionic emission velocity for holes and electrons is listed in Table. I. The initial equilibrium was solved while k_T equal to k_D .

IV. EXPERIMENT AND SIMULATION RESULTS

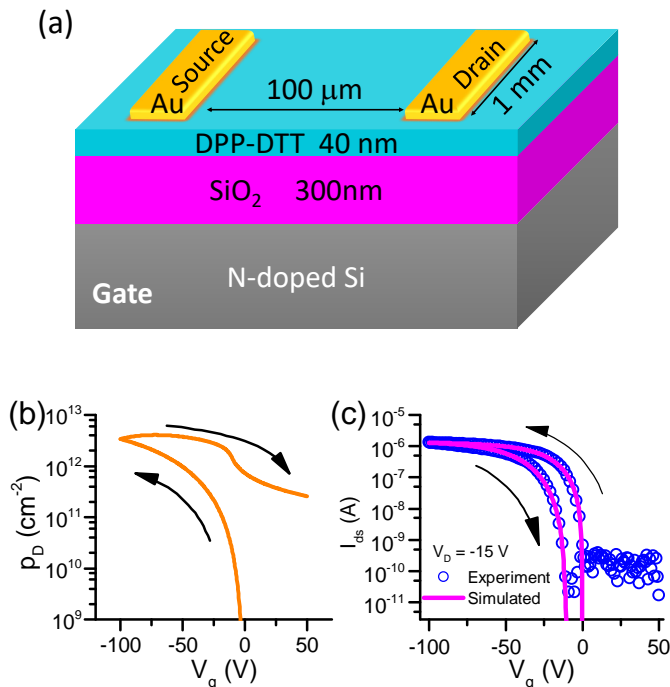


FIG. 6. (a) Schematic of the OTFT structure and layer composition. (b) The simulated DLT charge density versus gate bias. (c) The comparison of transfer characteristic between simulated and measured results. The arrows in (b) and (c) denote the sweeping direction of gate bias.

To examine our method, we fabricated a bottom-gate/top-contact OTFT by using DPP-DTT as active layer.

Fig. 6 (a) demonstrates the device structure. The architecture details are listed in Table. I. The DPP-DTT is an excellent p-type organic semiconductor material with high carrier mobility and stable chemical structure²³. Its energy levels are listed in Table. I. For the fabrication procedure, we first deposited its 5mg/ml chlorobenzene solution via spin-coating on a octyltrichlorosilane (OTS-8) treated Si/SiO₂ substrate. Then, 100nm gold layers were thermal evaporated using a shadow mask as source and drain electrodes. The electrical measurements for this OTFT was carried out by a Keithley 4200 semiconductor analyzer in atmosphere. The source contact was grounded and the drain bias was set to -15 V. The gate bias was first swept forwardly from 50 V to -100 V, then swept back to 50 V. The sweeping speed of gate bias was 10 V/s.

Both measured and simulated results are showed in Fig. 6 (b) and (c). All of simulation parameters are listed in Table I. In Fig. 6(b), the DLT charges increase while the device is driven to hole accumulation regime with enough negative gate bias. But as a nonequilibrium process, the trap concentration did not synchronize with the gate bias. The maximum point for DLT charges occurs around -60 V while sweeping the gate bias back to 50V. Fig. 6(c) presented the simulated and measured transfer characteristic curves. Due to the accumulation of trapped DLT charges, the drain current in backward scan is smaller than that in forward scan. So, the Transfer curves present an anti-clockwise hysteresis loop and the threshold voltage shifts about -16 V in the backward scan.

V. CONCLUSION AND FUTURE WORK

We have combined theoretical framework of the trapping and detrapping pictures in organic semiconductors that comprise two Gaussian DOSs. Through the introducing of EES for DLT and EFS for HOMO, both trapping and detrapping expression were reduced to two simple product forms. This model is demonstrated in a FVM based device simulator. To verify this model, we fabricated a DPP-DTT based TFT with bottom-gate/top-contact configuration. The good agreement of the simulated and experimental results testify the reasonability of this model. A more detailed analysis on charge trapping is a subject for further investigation.

ACKNOWLEDGEMENTS

This work is granted by the Natural Science Foundation of Guizhou Province (No. QKHJC-ZK[2021]YB329 and QKHJC-ZK[2021]YB018). We thanks Mr. Wenxuan Qiu for his language support.

¹D. N. Congreve, J. Lee, N. J. Thompson, E. Hontz, S. R. Yost, P. D. Reusswig, M. E. Bahlke, S. Reineke, T. Van Voorhis, and

- M. A. Baldo, "External quantum efficiency above 100singlet-exciton-fission-based organic photovoltaic cell," *Science* **340**, 334–337 (2013).
- ²F. J. Lin, C. Guo, W. T. Chuang, C. L. Wang, Q. Wang, H. Liu, C. S. Hsu, and L. Jiang, "Directional solution coating by the chinese brush: A facile approach to improving molecular alignment for high-performance polymer tfts," *Adv Mater* **29** (2017), 10.1002/adma.201606987.
- ³Q. Zhao, H. Wang, Z. Ni, J. Liu, Y. Zhen, X. Zhang, L. Jiang, R. Li, H. Dong, and W. Hu, "Organic ferroelectric-based 1t1t random access memory cell employing a common dielectric layer overcoming the half-selection problem," *Adv Mater* **29** (2017), 10.1002/adma.201701907.
- ⁴A. K. Pandey and J.-M. Nunzi, "Rubrene/fullerene heterostructures with a half-gap electroluminescence threshold and large photovoltage," *Advanced Materials* **19**, 3613–3617 (2007).
- ⁵M. Gross, D. C. Müller, H.-G. Nothofer, U. Scherf, D. Neher, C. Bräuchle, and K. Meerholz, "Improving the performance of doped π -conjugated polymers for use in organic light-emitting diodes," *Nature* **405**, 661–665 (2000).
- ⁶M. Pfeiffer, K. Leo, X. Zhou, J. Huang, M. Hofmann, A. Werner, and J. Blochwitz-Nimoth, "Doped organic semiconductors: Physics and application in light emitting diodes," *Organic Electronics* **4**, 89–103 (2003), high Efficiency Light Emitters.
- ⁷A. Hagfeldt, G. Boschloo, L. Sun, L. Kloo, and H. Pettersson, "Dye-sensitized solar cells," *Chemical reviews* **110**, 6595–6663 (2010).
- ⁸I. Paci, J. C. Johnson, X. Chen, G. Rana, D. Popovic, D. E. David, A. J. Nozik, M. A. Ratner, and J. Michl, "Singlet fission for dye-sensitized solar cells: Can a suitable sensitizer be found?" *Journal of the American Chemical Society* **128**, 16546–16553 (2006).
- ⁹K. Ya-Chin, K. Tsu-Jae, and H. Chenming, "Charge-trap memory device fabricated by oxidation of si/sub 1-x/ge/sub x," *IEEE Transactions on Electron Devices* **48**, 696–700 (2001).
- ¹⁰H.-W. Lin, W.-Y. Lee, and W.-C. Chen, "Selenophene-dpp donor-acceptor conjugated polymer for high performance ambipolar field effect transistor and nonvolatile memory applications," *J. Mater. Chem.* **22**, 2120–2128 (2012).
- ¹¹H. F. Haneef, A. M. Zeidell, and O. D. Jurchescu, "Charge carrier traps in organic semiconductors: a review on the underlying physics and impact on electronic devices," *Journal of Materials Chemistry C* **8**, 759–787 (2020).
- ¹²R. A. Street, M. Schoendorf, A. Roy, and J. H. Lee, "Interface state recombination in organic solar cells," *Physical Review B* **81**, 205307 (2010).
- ¹³X. Zhan, A. Facchetti, S. Barlow, T. J. Marks, M. A. Ratner, M. R. Wasielewski, and S. R. Marder, "Rylene and related dimides for organic electronics," *Advanced Materials* **23**, 268–284 (2011).
- ¹⁴M. Bouhassoune, S. L. M. v. Mensfoort, P. A. Bobbert, and R. Coehoorn, "Carrier-density and field-dependent charge-carrier mobility in organic semiconductors with correlated gaussian disorder," *Organic Electronics* **10**, 437–445 (2009).
- ¹⁵R. Coehoorn, W. F. Pasveer, P. A. Bobbert, and M. A. J. Michels, "Charge-carrier concentration dependence of the hopping mobility in organic materials with gaussian disorder," *Physical Review B* **72** (2005), 10.1103/PhysRevB.72.155206.
- ¹⁶G. Chen and Z. Xu, "Charge trapping and detrapping in polymeric materials," *Journal of Applied Physics* **106** (2009), 10.1063/1.3273491.
- ¹⁷H. A. Alghamdi, G. Chen, and A. S. Vaughan, "Simulation of the developed electro-thermal aging model based on trapping and detrapping process," 10.1109/CEIDP.2015.7352125.
- ¹⁸H. T. Nicolai, M. M. Mandoc, and P. W. M. Blom, "Electron traps in semiconducting polymers: Exponential versus gaussian trap distribution," *Physical Review B* **83** (2011), 10.1103/PhysRevB.83.195204.
- ¹⁹M. Scheb, C. Zimmermann, and C. Jungemann, "Field-induced detrapping in doped organic semiconductors with gaussian disorder and different carrier localizations on host and guest sites," *Physical Review B* **92** (2015), 10.1103/PhysRevB.92.104201.
- ²⁰J. M. Montero and J. Bisquert, "Interpretation of trap-limited mobility in space-charge limited current in organic layers with exponential density of traps," *Journal of Applied Physics* **110** (2011), 10.1063/1.3622615.
- ²¹W. C. Germs, J. J. M. van der Holst, S. L. M. van Mensfoort, P. A. Bobbert, and R. Coehoorn, "Modeling of the transient mobility in disordered organic semiconductors with a gaussian density of states," *Physical Review B* **84** (2011), 10.1103/PhysRevB.84.165210.
- ²²A. Miller and E. Abrahams, "Impurity conduction at low concentrations," *Physical Review* **120**, 745–755 (1960).
- ²³Y. Lei, P. Deng, M. Lin, X. Zheng, F. Zhu, and B. S. Ong, "Enhancing crystalline structural orders of polymer semiconductors for efficient charge transport via polymer-matrix-mediated molecular self-assembly," *Adv Mater* **28**, 6687–94 (2016).
- ²⁴DEVSIM LLC, "DEVSIM TCAD semiconductor device simulator," <https://devsim.org>.
- ²⁵M. Kimura, T. Nakanishi, K. Nomura, T. Kamiya, and H. Hosono, "Trap densities in amorphous- InGaZnO_4 thin-film transistors," *Applied Physics Letters* **92** (2008), 10.1063/1.2904704.
- ²⁶H. Xu, W.-J. Zhai, C. Tang, S.-Y. Qiu, R.-L. Liu, Z. Rong, Z.-Q. Pang, B. Jiang, J. Xiao, C. Zhong, B.-X. Mi, Q.-L. Fan, and W. Huang, "Thickness dependence of carrier mobility and the interface trap free energy investigated by impedance spectroscopy in organic semiconductors," *The Journal of Physical Chemistry C* **120**, 17184–17189 (2016).
- ²⁷G. Paasch and S. Scheinert, "Charge carrier density of organics with gaussian density of states: Analytical approximation for the gauss-fermi integral," *Journal of Applied Physics* **107** (2010), 10.1063/1.3374475.
- ²⁸D. A. Neamen, *Semiconductor physics and devices* (McGraw-Hill higher education, 2003).
- ²⁹J. O. Oelerich, D. Huemmer, and S. D. Baranovskii, "How to find out the density of states in disordered organic semiconductors," *Phys Rev Lett* **108**, 226403 (2012).
- ³⁰E. Knapp, R. Häusermann, H. U. Schwarzenbach, and B. Rühlstaller, "Numerical simulation of charge transport in disordered organic semiconductor devices," *Journal of Applied Physics* **108** (2010), 10.1063/1.3475505.
- ³¹A. Boubaker, B. Hafsi, K. Lmimouni, and A. Kalboussi, "A comparative tcad simulations of a p-and n-type organic field effect transistors: field-dependent mobility, bulk and interface traps models," *Journal of Materials Science: Materials in Electronics* **28**, 7834–7843 (2017).
- ³²S. D. Baranovskii, "Mott lecture: Description of charge transport in disordered organic semiconductors: Analytical theories and computer simulations," *physica status solidi (a)* **215** (2018), 10.1002/pssa.201700676.
- ³³J. Li, Y. Zhao, H. S. Tan, Y. Guo, C. A. Di, G. Yu, Y. Liu, M. Lin, S. H. Lim, Y. Zhou, H. Su, and B. S. Ong, "A stable solution-processed polymer semiconductor with record high-mobility for printed transistors," *Sci Rep* **2**, 754 (2012).
- ³⁴T. Ishibashi, "Chapter 5 - gaas-based and inp-based heterostructure bipolar transistors," in *Semiconductors and Semimetals*, Vol. 41, edited by R. A. Kiehl and T. C. L. G. Sollner (Elsevier, 1994) pp. 291–358.
- ³⁵M. Ghittorelli, T. Lenz, H. Sharifi Dehsari, D. Zhao, K. Asadi, P. W. M. Blom, Z. M. Kovacs-Vajna, D. M. de Leeuw, and F. Torricelli, "Quantum tunnelling and charge accumulation in organic ferroelectric memory diodes," *Nature Communications* **8**, 15741 (2017).
- ³⁶"Metal-insulator-semiconductor capacitors," in *Physics of Semiconductor Devices* (2006) pp. 197–240.